Robotic Bronchoscopy System with Variable-Stiffness Catheter for Pulmonary Lesion Biopsy

Xing-Yu Chen[1,2,3], Wenjie Lai[2,3], Xiaohui Xiong[1], Xuemiao Wang[1], Shi-Mei Wang[1], Peng Li[1], Weiyi Han[1], Yangyang Du[1], Wenke Duan[1], Wenjing Du[1], Soo Jay Phee[2,3], and Lei Wang[1,*]

***Abstract*—Bronchoscopy is a minimally invasive and effective method for early lung cancer diagnosis. Traditional bronchoscopy faces challenges such as limited dexterity, operator fatigue, and difficulty in maintaining steady manipulation. Existing robot-assisted methods have deficiencies, such as tool instability due to the dynamic respiratory environment. This paper presents a teleoperated robotic bronchoscopy system, featuring a controllable variable-stiffness catheter that enhances stability and flexibility during transbronchial biopsies. The 7 DoF robotic system allows for translation, rotation, and bending of the bronchoscope; delivery and bending of the catheter; delivery and control of biopsy tools; as well as stiffness adjustment of the catheter, which adapts to the dynamic pulmonary environment to provide stable support during tissue sampling. Key contributions include the robotic platform integrated with the variable-stiffness catheter and the implementation of a novel three-stage procedure for tissue sampling. The robotic system has been thoroughly evaluated through a series of tests, including the system accuracy, characterization of the variable-stiffness catheter's flexibility, force exertion, safety during operation, temperature control, and in-vivo experiment. The results demonstrated the system's feasibility and effectiveness, with metrics such as safe force limits, system flexibility, and positioning accuracy, showing its potential to improve the accuracy and safety of traditional bronchoscopy procedures.**

***Index Terms*—Robotic bronchoscopy, Surgical Robots, Variable Stiffness Catheter**

I. Introduction

Lung cancer remains one of the most prevalent and lethal forms of cancer worldwide, characterized by high morbidity and mortality rates [1]. Early detection is crucial in improving the survival prospects of lung cancer patients. Diagnostic approaches such as bronchoscopy and percutaneous needle biopsies are pivotal [2]. The percutaneous needle biopsy involves inserting a needle through the chest skin into the lung to extract tissue samples. However, this method is associated with significant risks of complications, including pneumothorax and considerable bleeding [3]. Transbronchial biopsy, facilitated by a flexible bronchoscope inserted through the bronchus, presents a minimally invasive alternative that mitigates these risks. This procedure utilizes real-time video imaging from the bronchoscope to navigate the complex bronchial pathways and accurately target lung lesions. Specialized instruments, such as biopsy forceps and biopsy needles introduced through the bronchoscope's working channel, enable the precise collection of pathological tissue samples for thorough analysis [4]. This method reduces the risk of procedural complications and provides a strategic advantage in the early diagnosis and treatment of lung cancer.

Robot-assisted bronchoscopy for the diagnosis and treatment of peripheral pulmonary lesions has recently gained favor among surgeons and scholars [5]–[8]. Robotic technology, with enhanced precision, spatial flexibility, and dexterity, has the potential to improve minimally invasive surgeries and the navigation of surgical tools for transluminal interventions [9]. Robot-assisted surgery can replace human hands, providing surgeons with a clearer view during operations, more precise tool delivery, and a more delicate sense of haptic feedback [10]. The Monarch™ platform from Auris Health (Redwood City, USA) features an inner bronchoscope (4.2 mm, with a 2.1 mm working channel) and an outer catheter (6 mm) with electromagnetic guidance for teleoperation [11]. The outer sheath can articulate up to 130 degree, allowing the bronchoscope to advance further into the periphery [12]. Intuitive Surgical's Ion™ endoluminal system (Sunnyvale, USA) is another renowned bronchoscopy platform utilized for peripulmonary nodule interventions. The bronchoscope has a 3.5 mm outer diameter with a 2 mm working channel, and the catheter can articulate up to 180 degree in any direction, controlled by a ball mouse and scroll wheel. Noah Medical (San Carlos, USA) developed the Galaxy™ system with tomosynthesis and electromagnetic navigation to provide real-time navigation and updates on lesions during lung interventions [7]. The Galaxy™ system features a bronchoscope with a 4.0 mm outer diameter and a 2.1 mm working channel.

Although these systems have demonstrated certain clini-

This work is supported by National Natural Science Foundation of China (U21A20480). This research is partially supported by grant (021990-00011) from the National Research Foundation, Prime Minister's Office, Singapore under its Campus of Research Excellence and Technological Enterprise (CREATE) program.

[1] Shenzhen Institutes of Advanced Technology, Chinese Academy of Sciences, Shenzhen, China.

[2] School of Mechanical and Aerospace Engineering, Nanyang Technological University, Singapore.

[3] Singapore-HUJ Alliance for Research and Enterprise (SHARE), the Smart Grippers for Soft Robotics (SGSR) Programme, Campus for Research Excellence and Technological Enterprise (CREATE), Singapore.

Corresponding author: Lei Wang. Emails: chenxingyu.medical@gmail.com, wjlai@ntu.edu.sg, 1948492662@qq.com, jnuhanweiyi@163.com, dyy236scu@163.com, msjphee@ntu.edu.sg, (xh.xiong1; xm.wang2; sm.wang; p.li1; wk.duan; wj.du; wang.lei)@siat.ac.cn

cal efficacy, they are currently limited to controlling only a few biopsy tools, which restricts the clinical application potential of robotic bronchoscopy. Several challenges need to be addressed in future iterations and clinical adoption. A major challenge is precisely positioning biopsy tools in a dynamic environment influenced by the narrow pulmonary spaces, respiration, and heartbeat. Additionally, maintaining flexibility and precise control at the distal end of biopsy instruments within the confined spaces is crucial to enhancing the success rate of transbronchial diagnostics and treatment.

Inspired by the curved structures of natural orifices such as the airways, various novel soft biopsy instruments based on advanced soft materials, control modes, configuration schemes, and environmental sensing methods have been developed. These instruments can guide biopsy sampling tools to adapt to the curved deformations of the human body's natural passages, enabling access to the deeper periphery of the bronchial tree. However, due to the dynamic environment caused by lung respiration and heartbeat, soft biopsy tools are prone to various deformations and collisions within the spatially limited and narrow passages. Thus, it is essential to introduce stability mechanisms into soft biopsy instruments to ensure robustness in the positioning of biopsy tools.

Flexible medical devices with controllable stiffness technology have garnered considerable attention in recent years, leading to the development of various approaches to achieve variable stiffness [13]–[17]. Integrating controllable stiffness technology into minimally invasive surgical tools allows for real-time adjustment of stiffness properties and bending strength in different surgical scenarios. Soft biopsy instruments can more effectively navigate within natural orifices, while rigid biopsy instruments can perform various biopsy sampling actions more stably, unaffected by the external environment. Such biopsy tools with variable-stiffness ability have the potential to balance flexible control and stable support in the highly dynamic pulmonary environment.

The working principles of variable-stiffness can be categorized into two types: structural and material-based approaches. Variable structural stiffness relies on changes in the structure's wall thickness or friction between different layers within the structure. However, due to their larger dimensions, these structures are often too bulky for use in the confined spaces of the human body [18]. Material-based variable stiffness is achieved through changes in material properties induced by thermal, chemical reactions, or electromagnetic fields. The principles include phase changing using low melting point materials such as waxes, alloys, or polymers [19], glass transitions such as shape memory materials or biomaterials, and rheological fluids such as electrorheological and magnetorheological fluids. Among these technologies, variable-stiffness tools based on thermally induced phase transitions has the potential to be miniaturized. For instance, Lussi et al. [20] achieved compliance control of a sub-millimeter continuous variable stiffness catheter through the variable phase change boundary in low melting point alloy, which is controlled by a radial temperature gradient. Similarly, Chautems et al. [21] proposed a magnetic continuum device with variable stiffness, where the tip is precisely shaped and controlled using an external magnetic field. The serial segments, consisting of low melting point alloy, can be independently softened through electrical current change. Although with great potential to improve clinical procedures, the magnetic actuation technique still has a long way to go before reaching medical requirements. For example, the imaging equipment and the magnetic-actuation platform should work collaboratively without mutual interference or physical collision. Current preclinical and clinical magnetic systems still tend to be bulky and complex, which is hard to be installed in the operating room [22]. Additionally, magnetic-controlled surgical robots may encounter electromagnetic interference issues in clinical environments, and thus they are incompatible with the magnetic tracking system and MRI environments.

To address the challenges of accurate positioning and flexible biopsy in the highly dynamic peripheral pulmonary environment, this paper introduces a novel design for a robotic bronchoscopy system integrated with a variable-stiffness catheter. This integration enhances precision and flexibility during transbronchial biopsies. The system allows for translation, rotation, and bending of the bronchoscope, delivery and bending of the catheter, delivery and control of biopsy forceps, as well as stiffness control of the catheter, which adapts to the dynamic pulmonary environment to provide stable support during tissue sampling. Key contributions of this work include the development of the robotic platform integrated with the variable-stiffness catheter and the implementation of a three-stage procedure for tissue sampling. This procedure comprises the initial insertion of a bronchoscope robot, dynamic adjustment of the variable-stiffness catheter, and robot-assisted tissue sampling. The prototype of robotic system has been fully developed, and its feasibility and practicality have been validated through in-vivo experiments.

II. Robotic Bronchoscopy Methods

A. System Overview

The system comprises a teleoperated surgical robot specifically designed for trans-respiratory diagnosis, incorporating a three-stage design scheme that includes a bronchoscope, novel variable-stiffness catheters, and biopsy forceps, as illustrated in Fig. 1. The robot is mounted on a 5 Degree of Freedom (DoF) passive robotic arm to achieve the appropriate angle of intervention. Surgeons use tablets as the remote control system to teleoperate the three endoscopic instruments, inserting them through the patient's trachea and utilizing them for precise movements. Employing a multi-operator strategy, the robot is controlled through a scheduling arrangement and weight distribution, allowing mentor surgeons and trainee surgeons to observe the same surgical site and collaboratively control the surgical instruments simultaneously. Compared to the surgeon console of the Da Vinci surgical robot [23], Force Dimension's haptic devices [24], and other custom-made master control units [10], this Human-Machine Interface (HMI) allows for quick integration of new features, making it convenient for

prototyping. However, it lacks physical feedback and cannot provide similar force feedback information, which may increase the risk of operational hazards. Prolonged use of the touchscreen may also cause fatigue in the fingers or hands of the surgeon. Additionally, there are security concerns in wireless environments. Future improvement will transfer the control algorithm to a more ergonomic surgeon console.

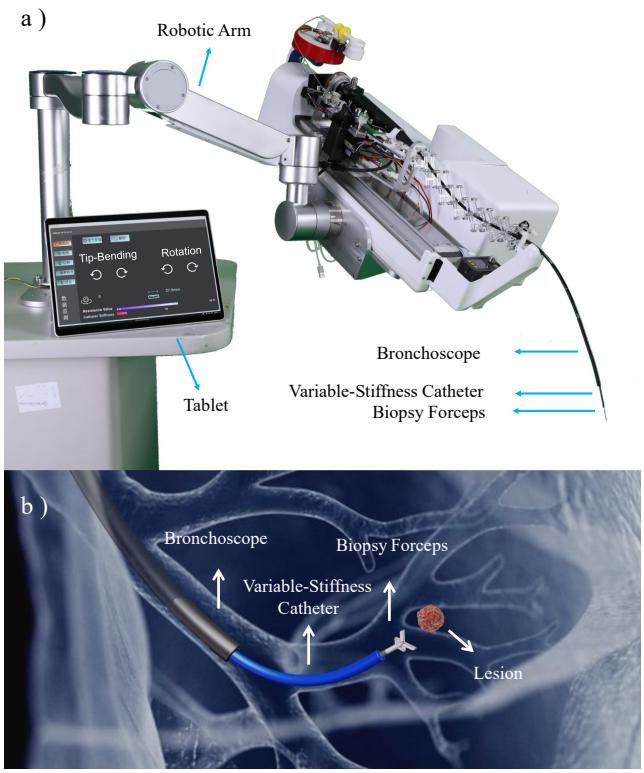

Figure 1. Structure of proposed robotic bronchoscopy system. a). System mounted on a robotic arm, with bronchoscope, variable-stiffness catheters, and biopsy forceps. b). Illustration of the three-stage biopsy method for lung lesion sampling.

Table I
ESSENTIAL MECHANICAL PARAMETERS.

Idx.	Endoscopic Instruments	Parameters	Size
1	Bronchoscope	Outside Diameter	5.2 mm
2	Bronchoscope	Inside Diameter	2.6 mm
3	Variable-Stiffness Catheter	Outside Diameter	2.4 mm
4	Variable-Stiffness Catheter	Inside Diameter	1.2 mm
5	Biopsy Forceps	Diameter	1.0 mm

Table I presents the essential mechanical parameters of the three-stage robotic bronchoscopy system. The size of the variable-stiffness catheter lies between that of the bronchoscope and the biopsy forceps, serving as the core component of the three-stage biopsy procedure. The variable-stiffness catheter is inserted through the working channel of the bronchoscope, and the biopsy forceps are subsequently inserted through the variable-stiffness catheter, as illustrated in Fig.1. The size of the variable-stiffness catheter is only half that of the bronchoscope, allowing it to navigate narrower bronchi and extend the reach of the biopsy forceps. Additionally, the variable-stiffness catheter provides stiffness support for the biopsy forceps within the dynamic environment of the lungs, accommodating the effects of respiration and heartbeat.

B. Design of Bronchoscope Robot

The robot is designed to replicate the operations performed by surgeons in traditional bronchoscopy biopsy procedures. The operating mechanism, as shown in Fig. 2 a), is divided into three levels of driving mechanisms. The first level completes the delivery, rotation, and tip bending of the bronchoscope. The system is compatible with commercial manual bronchoscope and easy to be plug in, it can be readily replaced by other flexible endoscopes for cost savings. The bronchoscope (UEWorld™, Zhejiang, China) has an external diameter of 5.2 mm and a working channel of 2.6 mm. The bronchoscope, with a length of 600 mm, is fixed to the platform using clips to enable horizontal delivery. A motor drives a worm screw that engages with a worm wheel, allowing the platform on the sliding table to rotate from 0 to 220 degrees. The bronchoscope tip controller is located beneath the bronchoscope, and the motor drives the bending stage to achieve the bending motion of the bronchoscope tip. It is capable of a 160-degree upward and 130-degree downward bending angle.

The second-stage driving mechanism shown in Fig. 2 c) is used for the delivery and bending control functions of the variable-stiffness catheter. The catheter delivery operation employs a friction wheel drive method. The delivery motor drives the driving wheel and the driven wheel to achieve forward and reverse movement of the catheter through friction. The distance between the driven and driving wheels is flexibly adjustable using a delivery clamping device. The clamping force between the driving and driven wheel can be adjusted by installing springs of different hardness. The bending motion of the catheter tip is driven by a bending motor. The catheter bending tendon is fixed to the bending slider, and the rotation of the bending motor causes the bending slider to move along the bending guide rail. This movement drives the catheter to bend, thereby enabling the variable-stiffness section at the catheter tip to perform controlled bending actions. An electric gripper is used to secure the catheter during bending, ensuring the stability of the catheter's position.

The third-stage driving mechanism forceps container shown in Fig. 2 b) is responsible for the delivery and opening or closing actions of the biopsy forceps. The 1 mm diameter biopsy forceps are attached to the forceps container and wrapped around the grooves below. The forceps container can rotate, and the telescopic motor above controls the biopsy forceps. The motor wires are connected through an internal conductive slip ring.

C. Multimodal Navigation System

Bronchoscopic images provide the most intuitive visual information, reflecting the internal condition of the lungs

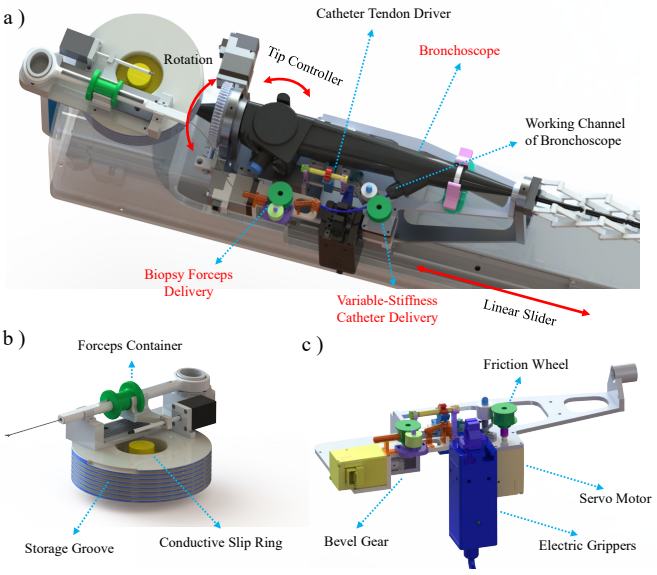

Figure 2. Structure of the bronchoscope robot. a) Top view of the control mechanism. b) Forceps container, to store the long biopsy forceps and control its opening and closing. c) Friction wheels to delivery the variable-stiffness catheter and biopsy forceps.

in real-time. However, due to their first-person perspective, these images do not reveal the bronchoscope's position within the lungs. To address this limitation, the robot employs a multimodal navigation system, which includes bronchoscopic videos, electromagnetic (EM) sensors, and C-Arm fluoroscopy.

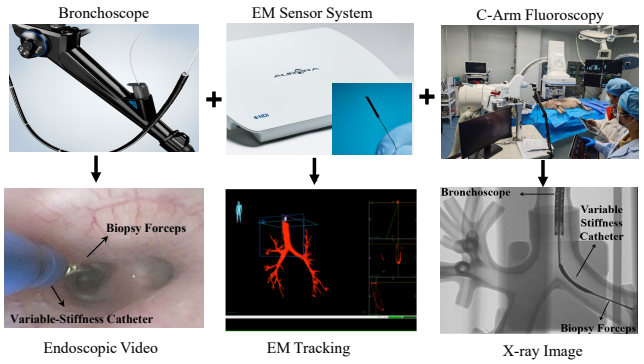

Figure 3. Navigation system workflow. Three-stage bronchoscopy surgical procedure composed of robotic bronchoscope, variable-stiffness catheter, and tissue sampling by biopsy forceps.

A 6-DoF EM sensor with position accuracy of 0.48 mm and orientation accuracy of 0.30° from Northern Digital Inc. is attached to the tip of bronchoscope to enable real-time navigation and tracking of the surgical instruments. This sensor provides information about the spatial position and orientation (roll, pitch, and yaw) of the bronchoscope. A field generator placed beside or under the patient generates an EM field of known geometry. As the EM sensor moves within this field, its spatial position and orientation are measured. The open-source software 3D Slicer is used to visualize the spatial position and orientation of the bronchoscope within lungs, as shown in Fig. 3.

Hounsfield Unit (HU) values for many metals and alloys are higher than those of the human body [25] [26], making fluoroscopic X-ray particularly suitable for positioning the biopsy forceps and variable-stiffness catheter with low melting point alloy, especially during the clamping action in biopsy procedures. In the C-Arm medical imaging system, the X-ray generator and detector are positioned on a C-shaped arm, directly opposite and centrally aligned with each other. The C-Arm fluoroscopy system is capable of controlled rotation, allowing for imaging from various angles and positions.

D. Three-stage robotic bronchoscopy procedure

A novel three-stage robotic bronchoscopy procedure proposed in Fig. 4 involves the control of the bronchoscope, variable-stiffness catheter, and biopsy instruments. The surgery includes three types of operations: individual device control, dynamic adjustment, and biopsy procedure. In the first step, surgeons use tablets to navigate the bronchoscope robot to the target position, involving motions such as delivery, rotation, and tip bending. In the second step, the variable-stiffness catheter is heated and maintained at a safe temperature of 53°C to decrease its stiffness. Subsequently, the softened catheter is inserted through the bronchoscope's working channel. Its dynamic stiffness can be adjusted based on factors such as heartbeat and respiration. Compared to the bronchoscope, the variable-stiffness catheter can be inserted into narrower bronchi and offers more flexible control with the driving tendon. Once the softened catheter reaches the precise location of the targeted lesion, the current to the heating resistance wire is disconnected. This discontinuation of heat allows the low melting point alloy to cool naturally, restoring the catheter's stiffness.

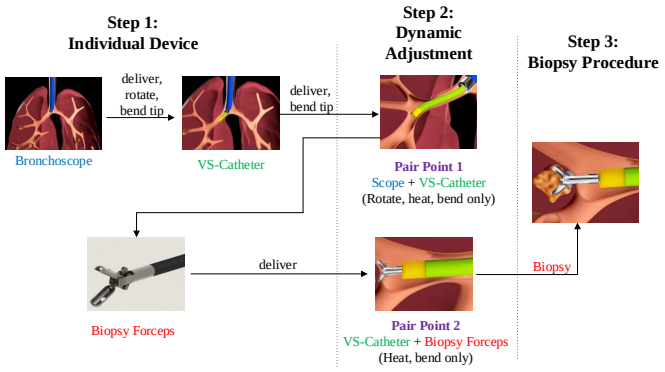

Figure 4. Multi-device collaboration of proposed robotic bronchoscopy.

Utilizing the concept of paired driving [27], the dynamic adjustment process of the robot has become a distinct driving mode. In our proposed system, once the bronchoscope reaches the appropriate position, only the rotation and bending control functions are allowed to fine-tune the direction of the variable-stiffness catheter. At this point, the catheter can be heated, bent, and delivered. After the variable-stiffness

catheter reaches the desired position, the delivery function of the catheter is paused, allowing only the biopsy forceps to be delivered. The variable-stiffness catheter retains only the heating and bending control functions to fine-tune the direction of the biopsy forceps.

Tissue sampling is then performed using the biopsy forceps. Surgeons can thereby examine the patient's airways, identify abnormalities or suspicious areas, and perform tissue biopsies for further testing. The entire three-stage process can be controlled using tablets, allowing surgeons to teleoperate the procedures. This highlights the importance of robotic surgery, as it enables surgeons to manipulate multiple medical tools without the need for shift changes, ensuring stability within the trachea.

III. Variable-Stiffness Catheter

A stiffness-controllable catheter is designed to enhance the stability of biopsy forceps within the dynamic environment of the lungs, as shown in Fig. 5. The catheter design aims to maintain optimal flexibility for seamless traversal of tortuous intraluminal pathways in the human body while ensuring sufficient rigidity to provide adequate support during tissue biopsy. The variable-stiffness catheter can be inserted into narrower bronchi and offers more flexible control with dynamic stiffness. The characteristics of the variable-stiffness catheter can be described in the following two states:

1) **Rigid State:** The variable-stiffness catheter is capable of withstanding tissue interaction forces under strong dynamic respiratory conditions, maintaining a stable posture and shape for biopsy forceps.
2) **Soft State:** The variable-stiffness catheter can adaptively navigate through the complex anatomical structures of the lungs, minimizing interaction forces with the inner wall of the bronchus and thereby reducing the risks associated with biopsy procedures.

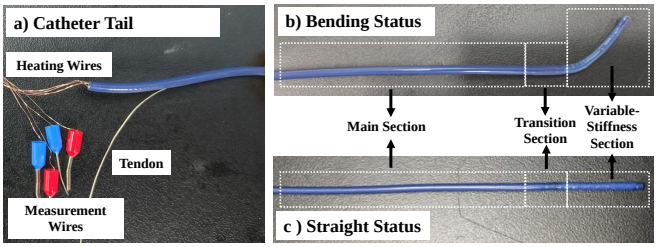

Figure 5. The variable-stiffness catheter example, consists of variable-stiffness section, transition section, main section, bending tendon, and tail.

A. Structure

The 850 mm catheter comprises five sections: the variable-stiffness section, transition section, main section, bending tendon, and tail, each varying in hardness according to its functional location. It features a hollow, tubular structure composed of multiple layers: an inner tube entirely of polytetrafluoroethylene (PTFE), an inner PEBAX® elastomer material layer, a phase change layer composed of low melting point alloy (LMPA), and an outer PEBAX layer, as illustrated in Fig. 6.

In the variable-stiffness section, a cylindrical cavity exists between the inner and outer PEBAX layers, filled with LMPA to achieve the catheter's variable stiffness. In other functional sections, the inner and outer materials are closely bonded. The outer material contains four independent cavities, distributed at 90° intervals, designated as the tendon chamber, heating wire chamber, and two measurement wire chambers.

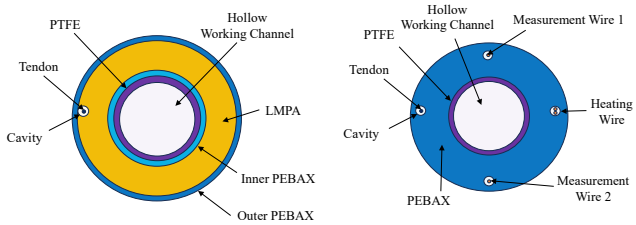

Figure 6. Structure of proposed variable-stiffness catheter.

1) Variable-Stiffness Section: The 30 mm variable-stiffness section of the catheter uses PEBAX material with a Shore hardness of 35D. This section is responsible for executing the catheter's bending and stiffness variation functions. It features LMPA filled between the inner and outer PEBAX walls. Copper heating wires are wound around the inner tube wall, and these heating wires, along with measurement wires, pass through the tail section of the catheter and are connected to the heating circuit and resistance measurement module with resolution of 0.1mΩ and accuracy of 0.1Ω, respectively. The heating circuit uses different voltage to generate controllable heat, adjusting the phase change of the LMPA to control the stiffness variation. The two measurement wires form a measurement circuit within the LMPA. As the alloy undergoes phase changes, the overall resistance of the measurement circuit dynamically changes.

2) Transition Section: The 10 mm transition section uses PEBAX 4533 elastomer material with a Shore hardness of 45D. The hardness of the transition section lies between that of the variable-stiffness section and the main section. The outer wall material of the variable-stiffness section uses soft PEBAX 3533 to minimize the impact of wall material on stiffness variation. The main section uses PEBAX 5533 to maintain a certain hardness, which is beneficial for the robot's control over the delivery of the catheter. This design prevents bending at the joint between the variable-stiffness section and the main section due to the sudden change in hardness. The variable-stiffness section is covered with a softer PEBAX material, while the main section, serving as the supporting structure of the catheter, is covered with a harder PEBAX material. Without a transition section, bending the catheter would cause it to bend at the joint between the variable-stiffness section and the main section, adversely affecting the surgical procedure.

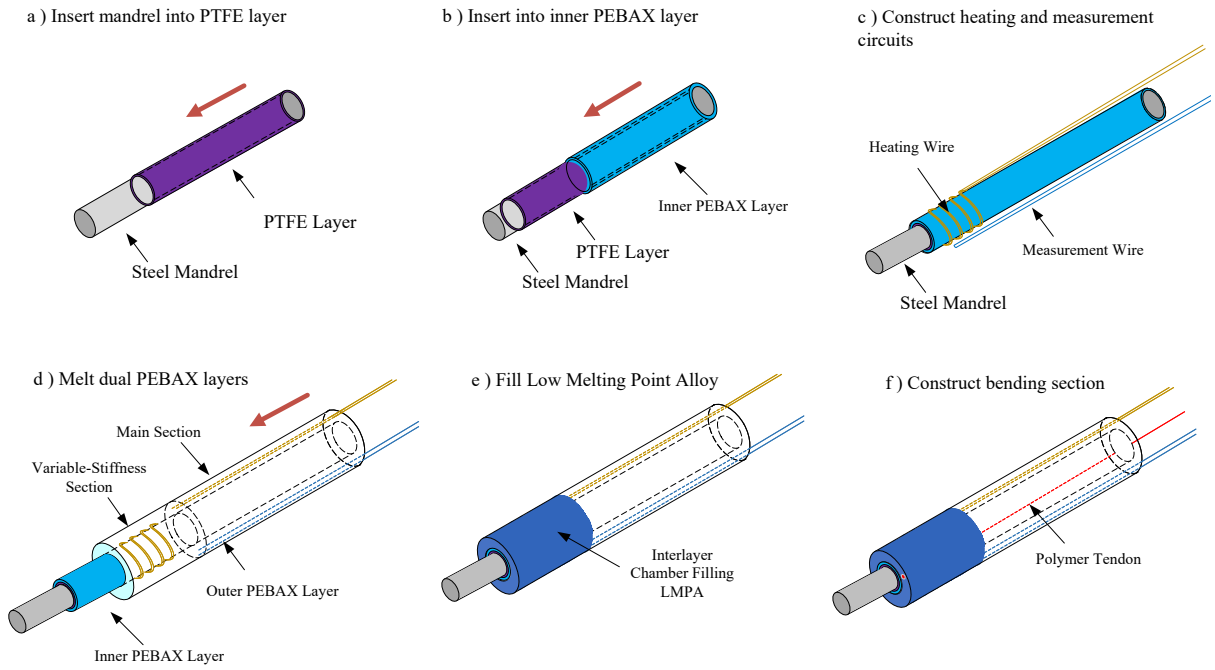

Figure 7. Manufacturing of the Variable-Stiffness Catheter.

3) Main Section: The main section utilizes PEBAX elastomer material with a Shore hardness of 55D and measures 800 mm in length, providing rigid support for the overall structure of the catheter. This section is integral to the catheter delivery mechanism, where the friction wheel force is applied. It relies on the friction between the friction wheel and the main section to deliver the catheter along the working channel of the bronchoscope.

4) Bending Tendon: The bending tendon of the catheter uses LCP wire with a diameter of 0.15 mm. The LCP wire is knotted and secured with a thin spacer at the tip of the catheter, serving as the fixed point for the bending force. The bending function of the catheter is independent of its variable stiffness function. The bending angle of the catheter is designed to range from 0° to 120°, with the bending tendon located in an independent pull-wire chamber. One end of the tendon is fixed at the tip of the catheter, while the other end is connected to an electric slider on the robot platform, which is driven by a motor to accomplish the bending function.

5) Tail Section: The 10 mm tail section is the part where the heating wire and measurement wire connect to the robot control system. It is made of the same material as the main section and is fixed to the catheter guide tube. The heating wires and measurement wires are distributed at 90° intervals. The heating wire adjusts the amount of heat generated to control the phase change speed of the LMPA, thereby controlling the stiffness of the catheter. The measurement wire is used to measure the resistance value of the measurement circuit during the phase change process of the LMPA.

Table II
PARAMETERS OF VARIABLE-STIFFNESS CATHETERS.

Idx.	Variable-Stiffness Catheter Parameters	Size
1	Outside Diameter	2.4 mm
2	Inside Diameter	1.2 mm
3	Overall Length	850 mm
4	Variable-Stiffness Length	30 mm
5	PTFE Thickness	0.05 mm
6	Inner PEBAX Thickness	0.05 mm
7	Outer PEBAX Thickness	0.10 mm
8	LCP Tendon Diameter	0.15 mm
9	Heating Wire Diameter	0.05 mm
10	Measurement Wire Diameter	0.10 mm
11	Turns of Heating Wire	14 turns
12	Exposed Measuring Wire Length	5 mm
13	LMPA Weight	0.56 g

B. Manufacture of Variable-Stiffness Catheter

Table II lists the essential parameters of the proposed variable-stiffness catheter. The inner tube is constructed from PTFE, with a wall thickness of 0.05 mm and a low friction coefficient of 0.05, facilitating the smooth passage of surgical instruments such as biopsy forceps. The other layers are composed of PEBAX, a material that offers the properties of thermoplastic elastomers, including precise dimensional stability, good resilience and recovery, and excellent fatigue resistance.

The process of manufacturing the variable-stiffness catheter

with LMPA is shown in Fig. 7, based on multilayer material lamination and polymer melting technology. Firstly, a slender steel rod with an outer diameter of 1.15 mm is used as the standard mandrel, onto which a layer of PTFE etched tube is fitted. A layer of PEBAX material is then coated onto the surface of the PTFE. Subsequently, copper wires are wound onto the inner PEBAX layer, a 5-chamber PEBAX material is fitted at the tail end, the copper wire is threaded through the outer PEBAX layer to construct the heating circuit and measurement circuit of the catheter. Next, LMPA is filled into the copper wire-wound section to achieve variable stiffness of the catheter based on the alloy's phase change state. Finally, LCP tendon is added to the tip of the catheter to construct the bending structure of the variable-stiffness section. After the steel mandrel is removed, the remaining hollow space serves as the working channel of the variable-stiffness catheter.

C. Work Principle

The LMPA in the catheter is composed of Cerrolow-117, which has a phase transition temperature of 47.22°C (117°F). At normal human body temperature, the LMPA remains in a solid state, thereby conferring high stiffness characteristics to the catheter. The heating resistance wires, made of 0.05 mm enameled copper wire, are helically wound along the inner tube to maximize the contact area with the LMPA. The measurement wires, made of 0.1 mm exposed enameled copper wire, are positioned at the head end to form a measurement circuit with the LMPA, which acts as a conductive material. The peripheral circuit connects to a precision resistance acquisition device, enabling real-time monitoring of resistance changes in the measurement circuit.

During the entry into bronchus, the LMPA is heated, causing the catheter to become soft and allowing it to navigate through intricate anatomical tissues. Once the catheter reaches the target lesion, the heating circuit is deactivated, allowing the catheter to cool down and regain its rigidity. This rigidity provides a stable working channel for biopsy tools, enhancing the precision and safety of the surgical procedure. After the biopsy is completed, the heating circuit is reactivated to soften the catheter once more. Subsequently, the surgical instruments, the variable-stiffness catheter, and the bronchoscope are sequentially withdrawn from the entry channel, thus completing the surgical procedure.

For safety reasons, alarm and protection methods are integrated into the control algorithm. Any abnormal resistance measurement triggers a warning to the main controller and interrupts the heating program. Two mechanisms are employed to secure the heating procedure: a fuse is installed in the heating circuit to prevent momentary high currents, and the intrinsic electrical characteristics of the variable-stiffness catheter prevent the accumulation of excessive heat. Due to higher impedance at the connection point between the variable-stiffness catheter and the heating module, the heat generated in the tail area is also higher. When the accumulated heat becomes excessive, the heating circuit in the tail end of the variable-stiffness catheter will melt first, leading to the interruption of the entire heating circuit. Consequently, the catheter ceases to generate heat, thereby avoiding excess heat accumulation and minimizing the risk to the patient.

D. Stiffness Analysis

According to outer PEBAX diameter of catheter r_{p1}, LMPA outer diameter r_o, LMPA inner diameter r_i, inner PTFE diameter r_{p0}, Young's modulus of solid LMPA E_s, Young's modulus of liquid LMPA E_l, and Young's modulus of PEBAX E_p, the moment of inertia of catheter in rigid state I_s and in soft state I_l [20] can be written as:

$$I_s = \frac{1}{4}\pi \left[\left(\frac{E_p}{E_s} r_{p1} + \left(1 - \frac{E_p}{E_s}\right) r_o \right)^4 \right. \tag{1}$$

$$\left. + \left(\frac{E_p}{E_s} r_i + \left(1 - \frac{E_p}{E_s}\right) r_{p0} \right)^4 - r_i^4 - r_{p0}^4 \right] \tag{2}$$

$$I_l = \frac{1}{4}\pi \left[\left(\frac{E_p}{E_l} r_{p1} + \left(1 - \frac{E_p}{E_l}\right) r_o \right)^4 \right. \tag{3}$$

$$\left. + \left(\frac{E_p}{E_l} r_i + \left(1 - \frac{E_p}{E_l}\right) r_{p0} \right)^4 - r_i^4 - r_{p0}^4 \right] \tag{4}$$

the average Young's modulus in the rigid state $\overline{E_s}$ and the average Young's modulus in the soft state $\overline{E_l}$ of the catheter can be obtained as:

$$\begin{cases} \overline{E_s} = \frac{E_s(r_o^2 - r_i^2) + E_p\left[(r_{p1}^2 - r_o^2) + (r_i^2 - r_{p0}^2)\right]}{r_{p1}^2 - r_{p0}^2} \\ \overline{E_l} = \frac{E_l(r_o^2 - r_i^2) + E_p\left[(r_{p1}^2 - r_o^2) + (r_i^2 - r_{p0}^2)\right]}{r_{p1}^2 - r_{p0}^2} \end{cases} \tag{5}$$

the extreme value of the bending stiffness of the catheter is:

$$\begin{cases} K_{max} = \overline{E_s} I_s \\ K_{min} = \overline{E_l} I_l \end{cases} \tag{6}$$

By substituting the actual parameters of the catheter material into the formula, where the Young's modulus of PEBAX E_p is 21MPa, the Young's modulus of the solid LMPA E_s is 3.659 GPa [28], and the Young's modulus of the liquid LMPA E_l is 1.50 GPa [19], with the outer diameter of the PEBAX r_{p1} being 1.20 mm, LMPA outer diameter r_o being 1.10 mm, the LMPA inner diameter r_i being 0.70 mm, and the inner diameter of the PTFE r_{p0} being 0.60 mm, so we can obtain that K_{max} is 2348.48 $N \cdot mm^2$, and K_{min} is 343.68 $N \cdot mm^2$.

Therefore, the ratio of catheter's bending stiffness variation is:

$$\frac{K_{max}}{K_{min}} = 6.83 \tag{7}$$

This is the calculated stiffness variation, and the actual stiffness variation measured in Section IV.B, was found to be 6.82, which aligns with the calculated value. After the variable-stiffness catheter extends from the bronchoscope's working channel, it will be affected by the lung's respiratory movement, causing lateral forces on the catheter. The tip of

the catheter and the direction of biopsy forceps will oscillate along, which will impact the accuracy of tissue sampling. When the stiffness variation is large enough, the catheter in flexible state does not hinder the control of the biopsy forceps, while the catheter in rigid state can provide support during the biopsy process.

IV. Evaluation and In-vivo Experiments

A. Evaluation of Robotic System

The delivery accuracy of the proposed robotic bronchoscopy system is quantitatively measured, encompassing the delivery of the variable-stiffness catheter alone, the delivery of biopsy forceps alone, and both the rapid and slow delivery of the biopsy forceps within the variable-stiffness catheter, shown in Fig.8. Twenty runs of experiments were conducted in each category. Encoder data from the motor connected to the friction wheel, specifically the number of motor steps, were recorded by the motor driver. For each motor step change, the motor rotates by 0.36°, allowing for the calculation of the motor rotation angle. Given that the friction wheel diameter is 18 mm, the delivery distance corresponding to the rotation of the friction wheel can be determined.

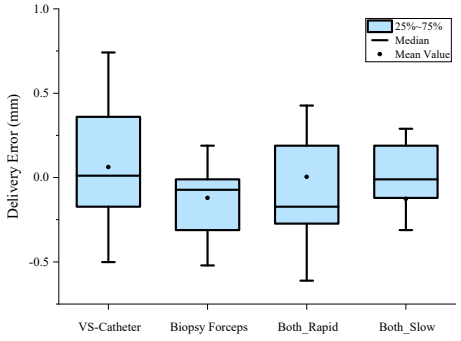

Figure 8. Delivery accuracy of variable-stiffness catheter and biopsy forceps.

The maximum delivery error for the variable-stiffness catheter was 0.741 mm, while for the biopsy forceps, it was 0.520 mm. This discrepancy arises from the rigidity of the biopsy forceps compared to the flexibility of the variable-stiffness catheter, leading to deformation during delivery. Additionally, when delivering the biopsy forceps inside the variable-stiffness catheter, the error noticeably increases compared to delivering the forceps alone. To address this issue, the delivery speed was reduced to one-fifth of the original speed, from 36°/s to 7.2°/s, thereby maintaining the delivery accuracy within 0.5 mm.

B. Catheter Flexibility Evaluation

Experiments were conducted to characterize the stiffness performance of the catheter. When the catheter extends its variable-stiffness section from the bronchoscope working channel, the force exerted on the catheter during the biopsy approximates that of a cantilever beam bending. The dynamic breathing of the lungs affects the catheter, causing it to oscillate continuously, which may impact the precision of lesion tissue sampling.

A miniature control medical tubing tester (QJ210-100 N, Qingji Instruments, Shanghai) was employed to conduct cantilever beam bending stiffness tests on the catheter. The variable-stiffness length of the catheter is 30 mm, so the catheter was extended by 20 mm from the bronchoscope's tip. The distributed load was converted into a concentrated load applied at the midpoint, 10 mm away from the tip of the bronchoscope. The experimental setup is depicted in Fig.9.

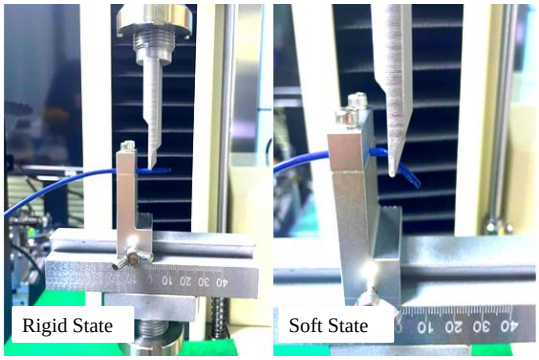

(a) Experimental setup. Left: Rigid Variable-Stiffness Catheter in rigid state with higher stiffness. Right: Variable-Stiffness Catheter in soft state with lower stiffness.

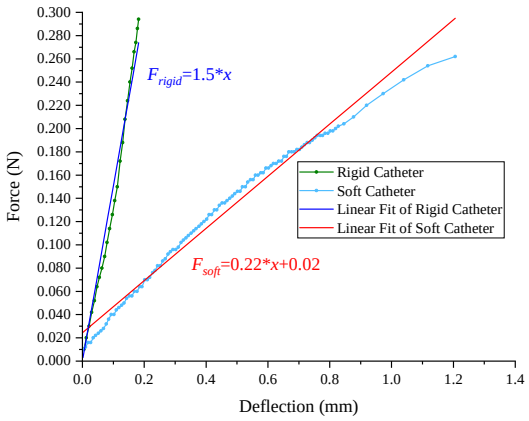

(b) Force-deflection curve of the variable-stiffness catheter in rigid and soft states.

Figure 9. Cantilever beam bending stiffness experiment.

The program applies a concentrated load moving downward at a speed of 0.1 N/s, testing the catheter in both rigid and soft states. This process yields force-deflection curves for both the rigid and soft states of the catheter. Data fitting is performed separately for each state, resulting in the following fitting formulas:

$$F_{rigid} = 1.5 * x \tag{8}$$

$$F_{soft} = 0.22 * x + 0.02 \tag{9}$$

The experiment yielded a stiffness-to-flexibility ratio $K = 1.5/0.22 = 6.82$ for the variable-stiffness catheter, which

aligns closely with the theoretically calculated result of 6.83 in Eq. 7.

C. Force characterization

Force experiments were also conducted in a bronchus phantom. A three-dimensional force sensor (SBT872, SIMBATOUCH, Guangzhou, China) was installed beneath the bronchus phantom to measure forces in the X, Y, and Z directions, as shown in Fig. 10. A robotic bronchoscopy procedure was completed on the force measurement platform with the bronchus phantom. It was observed that the maximum force occurs in the Y direction, horizontally to the right. When the bronchoscope tip collides with the bronchial bifurcation, the maximal force reaches 0.5 N. When the robot controls the bronchoscope tip to bend, a force in the -Y direction is applied backward to the model. The overall force remained below 0.5 N throughout the robotic bronchoscopy procedure, which is well below the axial applied force of 4.57 N observed during rigid bronchoscopy in patients' trials [29].

The forces exerted by the bronchoscope and the variable-stiffness catheter within the phantom were also measured. Both the bronchoscope and the variable-stiffness catheter were each delivered five times within the phantom, including one fast delivery and four slow deliveries. The slow speed is 1/5 of the fast speed. The force caused by the bronchoscope is significantly larger than that of the catheter, reaching 0.3 N during fast delivery. However, the force exerted by the catheter within the phantom remained relatively stable at 0.075 N, regardless of the delivery speed. This demonstrates that using the variable-stiffness catheter inside the bronchus, as opposed to using the bronchoscope, results in less impact on the patient's bronchus.

D. Safety Evaluation

Similarly, in the study of the axial stiffness validation experiment for the variable-stiffness catheter, the axial force generated by the catheter under tissue interaction was measured. The catheter's main structural segment was vertically fixed and tightened by a clamp to ensure that the variable-stiffness section remained in a stress-free state, being subjected only to axial pressure during the experiment. The load moves downward at a rate of 0.1 N/s until a fracture protection mechanism was triggered, as shown in Fig. 11.

The measured axial force-deformation curves for the variable-stiffness catheter in both rigid and soft states are shown in Fig.11 (b). In the rigid state, the maximum axial force on the catheter is 4.278 N, while in the flexible state, the maximum axial force is 1.036 N, which is also below the axial applied force of 4.57 N observed during rigid bronchoscopy in patients' trials.

E. Temperature characterization

To achieve precise control of the variable-stiffness catheter temperature and to explore the mechanism of stiffness change, experiments on LMPA transitions were conducted. A voltage range of 6 to 12 V was used to heat the variable-stiffness

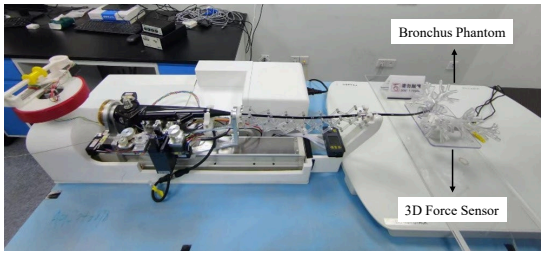

(a) Setup of force characterization of proposed robotic bronchoscopy system.

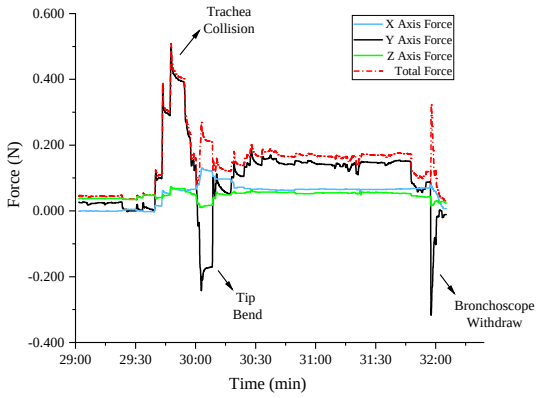

(b) Force measurement of bronchoscope in three dimension.

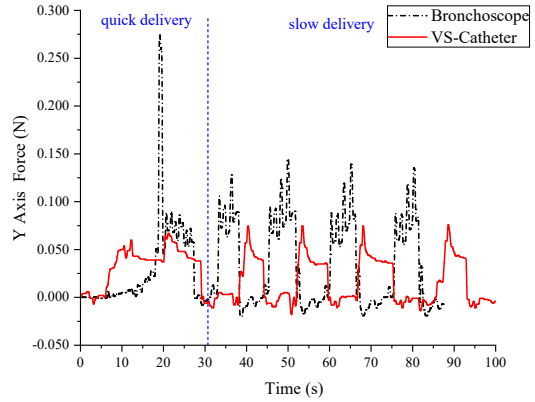

(c) Force measurement of bronchoscope and variable-stiffness catheter in different delivery speed.

Figure 10. Force characterization of bronchoscope and variable-stiffness catheter.

catheter, altering the rate and magnitude of heat generation in the heating circuit, in order to observe the conditions of alloy phase transitions, as shown in Fig. 12.

The initial temperature of the experiment was set to the normal human body temperature of 37°C. Different voltages ranging from 6V to 12V, with 1V intervals, were applied to heat the catheter, and a thermocouple was inserted inside the inner wall of the catheter tip for temperature measurement. Under the effect of the applied voltage, the heating circuit of the catheter generated resistive Joule heat, causing the temperature to rise rapidly. When the temperature reached the range of 47-48°C, the temperature curves under different voltages

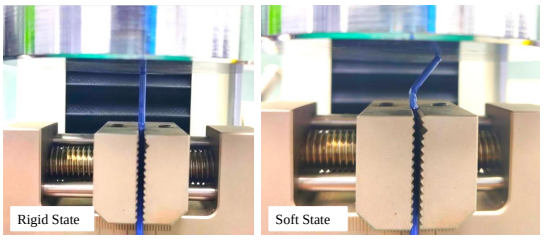

(a) Experiment setup. Left: Rigid Variable-Stiffness Catheter in rigid state with higher stiffness. Right: Variable-Stiffness Catheter in soft state with lower stiffness.

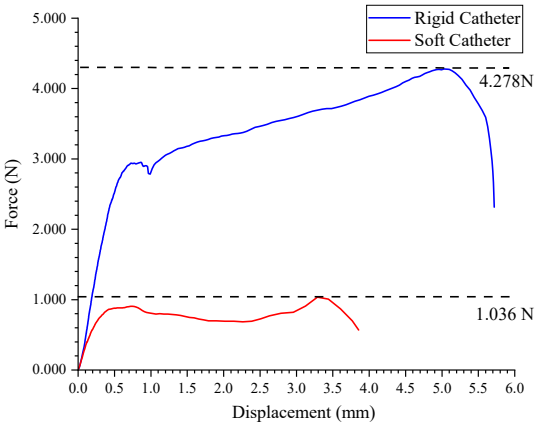

(b) Axial deformation relationship of variable-stiffness catheter in rigid and soft states.

Figure 11. Axial stiffness validation experiment for the variable-stiffness catheter.

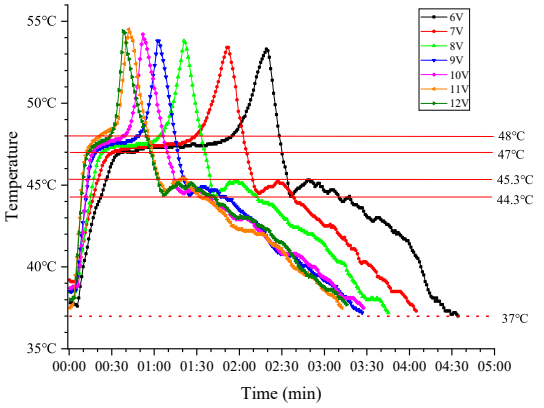

Figure 12. Temperature change with different heating voltages.

showed varying durations of temperature stabilization. This variation is due to the LMPA absorbing heat as it transitions from solid to liquid state:

$$Q = m \cdot \Delta H \tag{10}$$

where Q represents the amount of heat released or absorbed, m stands for the mass of the alloy, and ΔH denotes the specific latent heat for the LMPA.

Once the phase transition is complete and the alloy stops absorbing heat, the temperature resumes its pre-transition rate of increase, with the alloy fully transitioning to a liquid state, rendering the catheter flexible. When the temperature reaches 53°C, the heating circuit is deactivated to stop generating heat, allowing the catheter to cool naturally to the ambient temperature of the human body.

During the cooling process, the temperature briefly rises within the range of 44.3 to 45.3°C due to the alloy undergoing a phase transition from liquid back to solid. This process releases heat, as described by the phase transition equation 10, causing a temporary increase in temperature. Subsequently, the temperature gradually decreases again as the alloy completes its transition back to a solid state, and the catheter fully returns to a rigid state.

The heating process is significantly shorter than the cooling process, and this phenomenon becomes more pronounced as the heating voltage increases. Additionally, the rate of temperature decrease after the phase transition during the cooling process is noticeably slower compared to the rate before the transition.

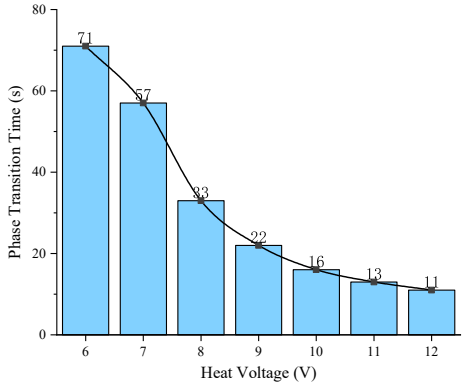

Figure 13. Phase transition time with variant voltages.

Under different voltages, the phase transition stages of the LMPA vary significantly, as shown in Fig. 13. At 6V, the phase transition stage lasts about 71s, while at 12V, it is reduced to 11s, indicating that the catheter rapidly completes the phase transition stage at higher voltages. This demonstrates that outside of the phase transition stage, the impact of voltage value is limited. To precisely control the temperature of the variable-stiffness catheter, it is necessary to flexibly adjust the voltage value during the phase transition stage of the catheter, rather than during the heating stage.

Fig. 14 shows the electrical resistance of the measurement circuit, which undergoes a rising-falling process. The higher the heating voltage, the faster the change in the electrical resistance of the variable-stiffness catheter, and the greater the maximum resistance value.

The results from the resistance and temperature experiments above indicate that the catheter's natural cooling rate in the high-temperature state is quite fast. This means that the system does not require an additional cooling system. Moreover, the catheter has a relatively long phase transition range, and by controlling the LMPA within the critical phase transition

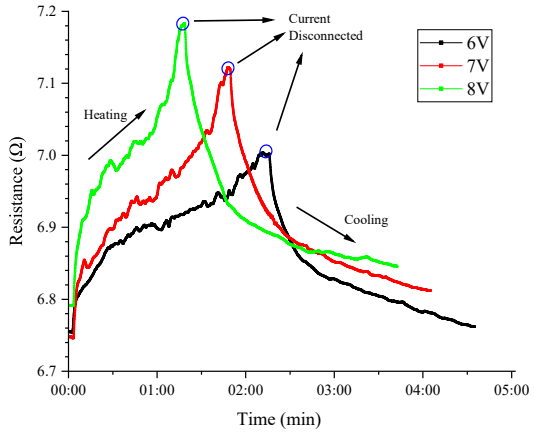

Figure 14. Resistance change of the measurement circuit.

range, it is possible to fast regulate the catheter's temperature and thus its stiffness. For this design, it is appropriate to balance control speed and safety by keeping the voltage controlled between 6 to 8V.

F. In-Vivo Experiment

The complete procedures of proposed system involve several steps, including preclinical CT scan, robot arm direction adjustment, bronchoscope robot controlling, and instruments retraction, as shown in Fig. 15. Following the setup and calibration of the robotic manipulator on the passive arm, the surgeon can remotely control the robotic system. During the robotic surgery, the respiratory and heart rate monitoring devices were installed first. Zoletil™ 50 was then used to induce anesthesia in the 26 kg pig. During the in-vivo experiment, propofol was administered via intravenous infusion to maintain anesthesia. After the installation and sterilization of the surgical robot, a fiducial EM sensor was attached to the pig's body surface, and another EM sensor was installed on the bronchoscope.

The three-stage structure composed of a bronchoscope, variable-stiffness catheter, and biopsy forceps was used to obtain tissue samples from the fourth and fifth level bronchi of the pig. Fig. 16 shows an bronchoscopic view of variable-stiffness catheter and biopsy forceps during the in-vivio experiment. Throughout the surgical procedure, the bronchoscope underwent rotation and advancement, the catheter was advanced, heated, and controlled for bending, and the biopsy forceps were advanced and used. Utilizing the variable-stiffness catheter, tissue samples were successfully obtained from the fourth and fifth level bronchi of the pig.

Postoperatively, a dissection was performed, and the excised bronchial tissue was sent for pathological examination. The results indicated no signs of burning in the lung tissue, confirming that the heating of the sheath did not damage the pig's trachea. Additionally, no scratches or frictional injuries were found in the remaining tracheal tissue, demonstrating that the entire robotic system caused no additional harm.

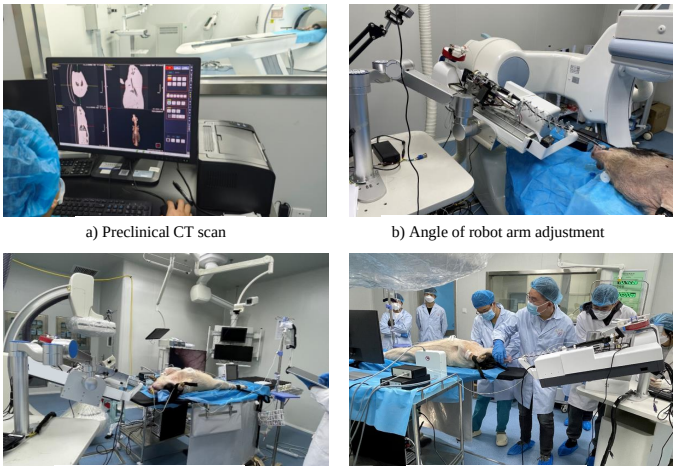

Figure 15. In-vivo experiment of proposed robotic system. a) Preclinical CT scan of the pig; b) robot arm direction adjustment; c) robotic bronchoscopy; d) instruments retraction.

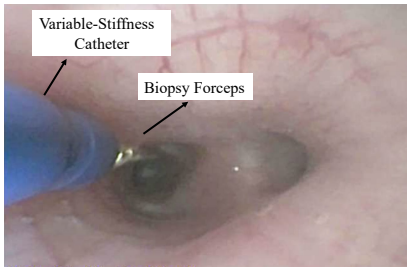

Figure 16. Bronchoscopic view of variable-stiffness catheter and biopsy forceps during in-vivo experiment.

V. Discussion and Future Works

This paper introduces a teleoperated robotic bronchoscopy system with variable-stiffness catheter to enhance the precision and flexibility for peripheral pulmonary lesion biopsy. The robotic system can replicate the operations performed by surgeons in traditional bronchoscopy procedures, including the control of bronchoscope and biopsy forceps, as well as the novel variable-stiffness catheter. The catheter can flexibly change its stiffness and alter direction within the working channel of bronchoscope. In rigid state, the variable-stiffness catheter can withstand tissue interaction forces under strong dynamic respiratory conditions and maintain stable posture and shape for biopsy forceps. In soft state, it can navigate through the complex anatomical structures of the lungs, minimizing interaction forces with the inner wall of the bronchus and risks during biopsy procedures. The experiments demonstrate the system's feasibility and effectiveness, showing its potential to improve the accuracy and safety of bronchoscopy procedures.

Experimental findings revealed that controlling the voltage allows for flexible adjustment of the catheter's temperature, thereby tuning its stiffness. However, the current manufacturing process of the catheter is not yet fully mature, re-

sulting in variations in the characteristics of each variable-stiffness catheter, such as the need to individually measure the resistance values of each one. Future work will focus on standardizing catheter performance, enabling consistent feedback on catheter temperature through resistance values. This will allow for the implementation of a PID algorithm to achieve precise control of stiffness. While the current system is designed to operate in a bistable mode for simplicity, we are investigating the possibility of implementing real-time stiffness control. This could allow for more adaptive and fine-tuned performance, depending on the needs of specific procedures.

When the flexible catheter contacts tissue, the deformation can be observed using X-ray imaging. Future work will also focus on investigating the palpation capabilities of the variable-stiffness catheter. By utilizing force feedback, the system aims to assess tissue abnormalities and diagnose potential pathological changes.

The experimental study has demonstrated the viability of the proposed robotic system and validated its design concept. Nevertheless, more comprehensive validation is necessary through thorough preclinical studies and additional in-vivo testing involving surgeons. These further evaluations will provide valuable insights into the system's practicality and effectiveness in actual surgical environments, ensuring its readiness for real-world applications.

ACKNOWLEDGMENTS

The study was approved by Institutional Review Board and Ethics Committee of Shenzhen Institutes of Advanced Technology (AAS 201205P).

REFERENCES

[1] R. L. Siegel, K. D. Miller, and A. Jemal, "Cancer statistics, 2018," *CA: a cancer journal for clinicians*, vol. 68, no. 1, pp. 7–30, 2018.

[2] R. Maconachie, T. Mercer, N. Navani, G. McVeigh, G. Committee *et al.*, "Lung cancer: diagnosis and management: summary of updated nice guidance," *Bmj*, vol. 364, p. l1049, 2019.

[3] J. Cicenia, S. K. Avasarala, and T. R. Gildea, "Navigational bronchoscopy: a guide through history, current use, and developing technology," *Journal of Thoracic Disease*, vol. 12, no. 6, p. 3263, 2020.

[4] R. Eberhardt, N. Kahn, D. Gompelmann, M. Schumann, C. P. Heussel, and F. J. Herth, "Lungpoint—a new approach to peripheral lesions," *Journal of thoracic oncology*, vol. 5, no. 10, pp. 1559–1563, 2010.

[5] L. Yarmus, J. Akulian, M. Wahidi, A. Chen, J. P. Steltz, S. L. Solomon, D. Yu, F. Maldonado, J. Cardenas-Garcia, D. Molena *et al.*, "A prospective randomized comparative study of three guided bronchoscopic approaches for investigating pulmonary nodules: the precision-1 study," *Chest*, vol. 157, no. 3, pp. 694–701, 2020.

[6] A. Agrawal, D. K. Hogarth, and S. Murgu, "Robotic bronchoscopy for pulmonary lesions: a review of existing technologies and clinical data," *Journal of thoracic disease*, vol. 12, no. 6, p. 3279, 2020.

[7] M. J. Diddams and H. J. Lee, "Robotic bronchoscopy: Review of three systems," *Life*, vol. 13, no. 2, p. 354, 2023.

[8] X. Duan, D. Xie, R. Zhang, X. Li, J. Sun, C. Qian, X. Song, and C. Li, "A novel robotic bronchoscope system for navigation and biopsy of pulmonary lesions," *Cyborg and Bionic Systems*, vol. 4, p. 0013, 2023.

[9] X. Chen, Y. Chen, W. Duan, T. O. Akinyemi, G. Yi, J. Jiang, W. Du, and O. M. Omisore, "Design and evaluation of a learning-based vascular interventional surgery robot," *Fibers*, vol. 10, no. 12, p. 106, 2022.

[10] W. Duan, Z. Li, O. M. Omisore, W. Du, T. O. Akinyemi, X. Chen, X. Gao, H. Wang, and L. Wang, "Development of an intuitive interface with haptic enhancement for robot-assisted endovascular intervention," *IEEE Transactions on Haptics*, 2023.

[11] J. Puchalski, "Robotic bronchoscopy for the diagnosis of peripheral lung nodules: a review," *Current Pulmonology Reports*, vol. 10, pp. 46–52, 2021.

[12] A. C. Chen, N. J. Pastis Jr, A. K. Mahajan, S. J. Khandhar, M. J. Simoff, M. S. Machuzak, J. Cicenia, T. R. Gildea, and G. A. Silvestri, "Robotic bronchoscopy for peripheral pulmonary lesions: a multicenter pilot and feasibility study (benefit)," *Chest*, vol. 159, no. 2, pp. 845–852, 2021.

[13] X. Wei, F. Ju, D. Bai, H. Guo, C. Lu, H. Wu, and B. Chen, "Design and compensation control of modular variable stiffness continuum manipulator for nasal surgery," *IEEE Transactions on Instrumentation and Measurement*, vol. 73, pp. 1–13, 2024.

[14] Y. Piskarev, J. Shintake, C. Chautems, J. Lussi, Q. Boehler, B. J. Nelson, and D. Floreano, "A variable stiffness magnetic catheter made of a conductive phase-change polymer for minimally invasive surgery," *Advanced Functional Materials*, vol. 32, no. 20, p. 2107662, 2022.

[15] J. Park, H. Lee, H. Kee, and S. Park, "Magnetically steerable manipulator with variable stiffness using graphene polylactic acid for minimally invasive surgery," *Sensors and Actuators A: Physical*, vol. 309, p. 112032, 2020.

[16] M. Mattmann, C. De Marco, F. Briatico, S. Tagliabue, A. Colusso, X.-Z. Chen, J. Lussi, C. Chautems, S. Pané, and B. Nelson, "Thermoset shape memory polymer variable stiffness 4d robotic catheters," *Advanced Science*, vol. 9, no. 1, p. 2103277, 2022.

[17] Y. Piskarev, Y. Sun, M. Righi, Q. Boehler, C. Chautems, C. Fischer, B. J. Nelson, J. Shintake, and D. Floreano, "Fast-response variable-stiffness magnetic catheters for minimally invasive surgery," *Advanced Science*, p. 2305537, 2024.

[18] H. M. Le, L. Cao, T. N. Do, and S. J. Phee, "Design and modelling of a variable stiffness manipulator for surgical robots," *Mechatronics*, vol. 53, pp. 109–123, 2018.

[19] B. E. Schubert and D. Floreano, "Variable stiffness material based on rigid low-melting-point-alloy microstructures embedded in soft poly (dimethylsiloxane)(pdms)," *Rsc Advances*, vol. 3, no. 46, pp. 24 671–24 679, 2013.

[20] J. Lussi, M. Mattmann, S. Sevim, F. Grigis, C. De Marco, C. Chautems, S. Pané, J. Puigmartí-Luis, Q. Boehler, and B. J. Nelson, "A submillimeter continuous variable stiffness catheter for compliance control," *Advanced Science*, vol. 8, no. 18, p. 2101290, 2021.

[21] C. Chautems, A. Tonazzini, Q. Boehler, S. H. Jeong, D. Floreano, and B. J. Nelson, "Magnetic continuum device with variable stiffness for minimally invasive surgery," *Advanced Intelligent Systems*, vol. 2, no. 6, p. 1900086, 2020.

[22] Z. Yang, H. Yang, Y. Cao, Y. Cui, and L. Zhang, "Magnetically actuated continuum medical robots: A review," *Advanced intelligent systems*, vol. 5, no. 6, p. 2200416, 2023.

[23] C. D'Ettorre, A. Mariani, A. Stilli, F. R. y Baena, P. Valdastri, A. Deguet, P. Kazanzides, R. H. Taylor, G. S. Fischer, S. P. DiMaio *et al.*, "Accelerating surgical robotics research: A review of 10 years with the da vinci research kit," *IEEE Robotics & Automation Magazine*, vol. 28, no. 4, pp. 56–78, 2021.

[24] R. V. Patel, S. F. Atashzar, and M. Tavakoli, "Haptic feedback and force-based teleoperation in surgical robotics," *Proceedings of the IEEE*, vol. 110, no. 7, pp. 1012–1027, 2022.

[25] S. A. Bolliger, L. Oesterhelweg, D. Spendlove, S. G. Ross, and M. Thali, "Is differentiation of frequently encountered foreign bodies in corpses possible by hounsfield density measurement?" *Journal of Forensic Sciences*, vol. 54, 2009.

[26] P. Mah, T. Reeves, and W. McDavid, "Deriving hounsfield units using grey levels in cone beam computed tomography," *Dentomaxillofacial Radiology*, vol. 39, no. 6, pp. 323–335, 2010.

[27] C. F. Graetzel, A. Sheehy, and D. P. Noonan, "Robotic bronchoscopy drive mode of the auris monarch platform," in *2019 International Conference on Robotics and Automation (ICRA)*. IEEE, 2019, pp. 3895–3901.

[28] R. Zhao, Y. Yao, and Y. Luo, "Development of a variable stiffness over tube based on low-melting-point-alloy for endoscopic surgery," *Journal of Medical Devices*, vol. 10, no. 2, p. 021002, 2016.

[29] L.-X. Barrette, M. Turkseven, S. De, A. Majid, M. Parikh, and A. Chee, "Characterization of applied forces and torques during rigid bronchoscopy intubation," *Journal of Bronchology & Interventional Pulmonology*, vol. 27, no. 4, pp. 246–252, 2020.